# Estimation of Shallow-Water Breaking-Wave Height From Synthetic Aperture Radar

Yuriy V. Goncharenko, *Member, IEEE*, Gordon Farquharson, *Member, IEEE*, Fengyan Shi, Britt Raubenheimer, and Steve Elgar

***Abstract*—The relationship between synthetic aperture radar (SAR) signatures of depth-limited breaking waves and wave height is studied. Wave height is estimated from SAR images using an empirically derived relationship that exploits the azimuthal shift in SAR images associated with moving scatterers. This relationship is derived from *in situ* measurements rather than from an idealized model of breaking waves as was done in a previous study. We find that the lengths of the SAR signatures are correlated with the observed significant wave height (the correlation coefficient is 0.78) for a range of wave conditions. The relationship between the wave heights and velocity bandwidths from the field data is similar to that between simulated (with a Boussinesq surface wave model) wave heights and velocity ranges (correlation coefficient $= 0.82$).**

***Index Terms*—Airborne radar, electromagnetic scattering, remote sensing, sea surface, synthetic aperture radar (SAR).**

## I. Introduction

DEPTH-limited ocean breaking waves have a clear and distinct signature characterized by bright streaks in along-track interferometric (ATI) synthetic aperture radar (SAR) imagery. Although many sensors have been used to obtan SAR imagery of nearshore waves [1], [2], only a few studies have examined the signatures of depth-limited breaking waves. These signatures are caused by orbital velocities in the breaking region that vary temporally (during the time the synthetic aperture is formed) and spatially, causing scatterers to map to different azimuthal positions in the image. While analytical models for the signature of depth-limited breaking waves suggest that the phase velocity of the wave is not directly related to the ATI SAR velocity measurement and therefore cannot be used to derive breaking-wave parameters directly [3], idealized model simulations of breaking waves suggest that the azimuthal displacements in SAR images allow estimation of depth-limited breaking-wave heights [4].

Manuscript received March 3, 2015; accepted April 9, 2015. This work was supported by the Fulbright Program and the Office of Naval Research.

Y. V. Goncharenko was with the Applied Physics Laboratory, University of Washington, Seattle, WA 98105 USA, and also with the Institute for Radiophysics and Electronics NAS of Ukraine, 61085 Kharkiv, Ukraine. He is now with the School of Electrical, Electronic and System Engineering, University of Birmingham, Birmingham B15 2TT, U.K. (e-mail: ygonch@brain.org.ua).

G. Farquharson is with the Air–Sea Interaction and Remote Sensing Department, Applied Physics Laboratory, University of Washington, Seattle, WA 98105 USA (e-mail: gordon@apl.uw.edu).

F. Shi is with the Center for Applied Coastal Research, University of Delaware, Newark, DE 19716 USA (e-mail: fyshi@udel.edu)

B. Raubenheimer and S. Elgar are with the Department of Applied Ocean Physics and Engineering, Woods Hole Oceanographic Institution, Woods Hole, MA 02543 USA (e-mail: braubenheimer2@whoi.edu-e; elgar@whoi.edu)

Digital Object Identifier 10.1109/LGRS.2015.2445492


Fig. 1. Antenna frame (arrow) installed on a Cessna 172. Both antennas radiate toward the starboard side of the aircraft.

In this letter, we show that the lengths of the SAR signatures are correlated with the observed significant wave height of depth-limited breaking waves estimated from *in situ* observations near the ebb shoal and neighboring beaches of New River Inlet, NC. The accuracy of the approach is assessed with Boussinesq wave model simulations. Although the approach to estimating depth-limited breaking-wave height is similar to that used previously [3], the development of the retrieval is significantly different, and the analysis of the results in terms of the model provides new information about the accuracy of the methodology. Other differences with [3] are that we relate the SAR signatures to significant wave height, as opposed to the trough to crest wave height, and we do not study the relationship between the SAR signature and depth.

## II. System Description

The remote field measurements were obtained with a miniaturized dual-beam ATI SAR [5] operated on a small aircraft (Fig. 1). The system is designed to measure surface velocity at high resolution using two dual-receiver frequency-modulated continuous-wave radars to implement dual-beam ATI SAR. The bandwidth of the transmitted signal is 80 MHz, so the slant range resolution is 1.875 m. The frequency bands of the radars are separated by 40 MHz, allowing the radars to operate simultaneously. The portside radar antennas are squinted forward of the side-looking (starboard) direction, and the starboard-side antennas are squinted backward (aft). The broadside-beam

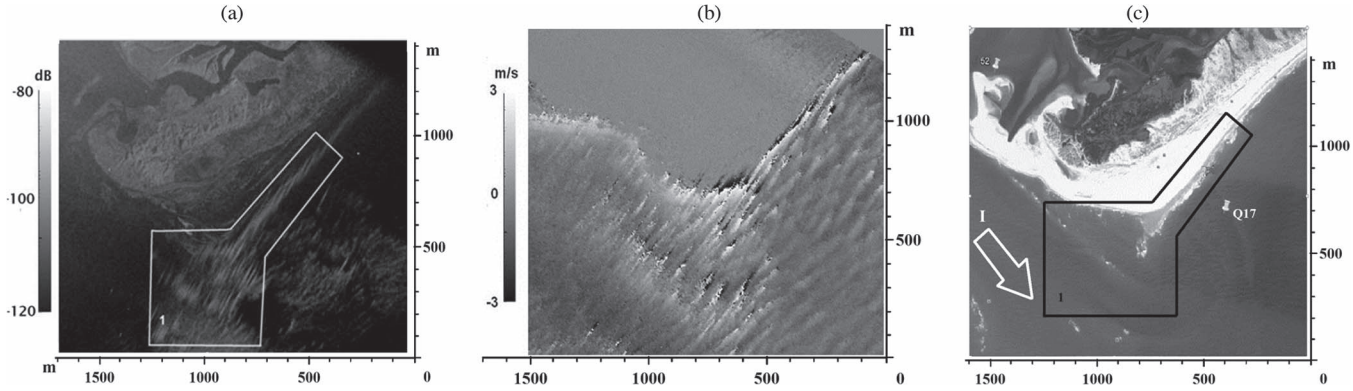


Fig. 2. Images of the experimental area. (a) SAR intensity image. (b) SAR velocity image. (c) Visible image with sensor location (Q17). The outlined polygons (labeled "1") in a and c indicate an area of depth-limited wave breaking. The white arrow ("I" in c) shows the inlet channel.

flat-panel antennas are mechanically rotated in the horizontal plane and tilted in the squinted plane. The squint angle is 30° measured in the horizontal plane, and the elevation angle is 60° measured in the plane defined by the propagation vector $\vec{k}$ and the $z$-axis. The antennas are not covered by a radome.

## III. Data

SAR data were collected along the North Carolina coast, adjacent to New River Inlet from May 1 to May 20, 2012 ($0 <$ wind speed $< 10$ m/s from the south or southwest, $0.3 <$ wave height $< 0.7$ m in 1–2 m water depth, wave direction normally incident $\pm 50°$, and tidal elevation range about 1 m). Although tidal flows are strong and can affect the waves, depth-limited breaking dominates in this region [6], producing strong wave breaking in 0–2 m water depth along the shoreline adjacent to the inlet and over the shoals just offshore of the inlet mouth [Fig. 2(a), white polygon]. The signatures of these breaking waves are visible in the SAR intensity and velocity images [Fig. 2(a) and (b)].

The surf zone wave heights were estimated with a pressure sensor buried beneath the sand surface (to reduce flow noise) about 150 m from the shoreline in 1–2 m water depth [Fig. 2(c)]. Significant wave heights ($H_{\mathrm{sig}}$, four times the standard deviation of sea-surface elevation fluctuations) were estimated from 512-s records using linear theory to convert the 2-Hz bottom pressure time series to sea-surface elevation. Offshore wave directions were estimated with buoy observations (NOAA 41110) in 16 m depth, 50 km to the south. As discussed in the following, the results are not sensitive to wave direction.

## IV. Signatures Of Breaking Waves

The azimuthal displacement in a SAR image of a moving scatterer from its true position is given by [7]

$$\Delta\mathcal{X} = \frac{R_0 V_r(\tan\theta\sin\theta + \cos\theta)}{V} \tag{1}$$

where $V_r$ is the velocity of the scatterer, $R$ is the range ($\sim$2000 m), $V$ is the aircraft velocity ($\sim$45 m/s), and $\theta$ is the squint angle of the radar. SAR images of complex features that consist of many scatterers with different velocities

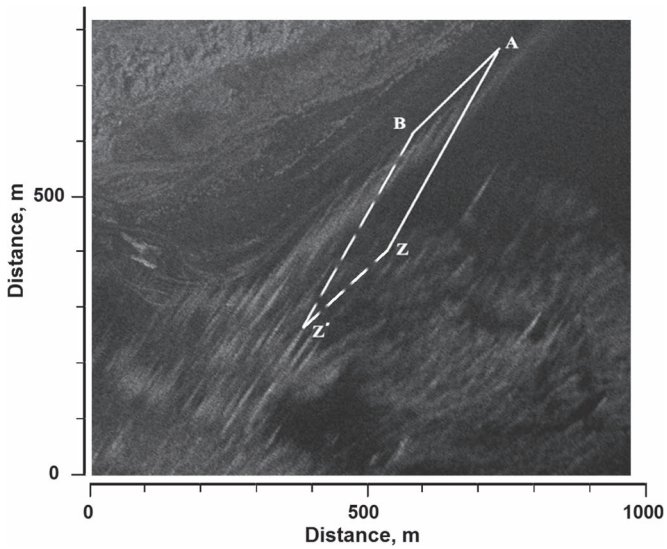


Fig. 3. Detailed intensity image of the surf zone. Line AB is the shoreline, and line AZ is the azimuthal direction.

(e.g., with many different $\Delta\mathcal{X}$) will include arcs with radius and length proportional to the bandwidth $\Delta V_r$ of the velocity distribution of the feature. The distance between each point of the arc and the real position of the target will correspond to the radial velocity of the elementary scatterer, and the intensity of this point will correspond to the radar cross section of this scatterer. If the arc radius is much larger than the length, the arc approximates a line (streak; Fig. 3). The bandwidth of surface velocities of breaking waves with $H_{\mathrm{sig}} \approx 1$ m can exceed 3 m/s [8], so the length of a streak can exceed 130 m. Although tidal currents are strong in the inlet channel ($\pm$ 1.5 m/s), mean flows were relatively weak on the shoals [6] and do not appear to affect the measurements. Thus, significant wave heights can be determined from the velocity bandwidths $\Delta V_r$ that are estimated from the lengths $L$ of the streaks owing to breaking waves.

In addition to the azimuthally broad signature, wave breaking causes an increase in backscattered power and sharp gradients in radial velocity in SAR images [9]. These intermittent and spatially variable breaking-wave processes occur during the

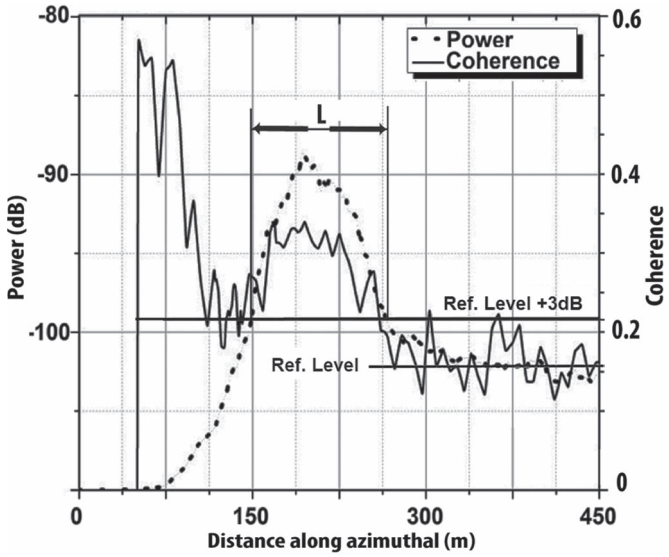


Fig. 4. Averaged intensity (dotted curve) and interferometric coherence coefficient (solid curve) of streaks versus distance along an azimuthal line (AZ in Fig. 3) on May 17, 2012, 13:12 UTC. The beach is between distances 0 and about 100 m, the surf zone is between 100 and 250 m, and seaward of the surf zone is from 250 to 450 m. The reference level corresponding to the backscattered signal from a surface without breaking waves (green line) and the power level (red line) used to estimate the streak length ($L$, red arrows, here about 120 m) are indicated.

time over which the synthetic aperture is formed, resulting in a reduction of the azimuthal resolution of the SAR image to [9]

$$\rho_{\text{flux}} = \frac{\lambda}{2\beta}\left[1+\left(\frac{\beta R}{V\tau}\right)^2\right]^{\frac{1}{2}} \tag{2}$$

where $\lambda$ is the electromagnetic wavelength ($\sim$0.07 m), $\beta$ is the antenna azimuthal beamwidth ($\sim$0.1 rad), and $\tau$ is the coherence time ($\sim 0.1-0.2$ s). However, even with this reduction, the resolution is better than 15 m, which is small compared with the signatures of breaking waves, so the effects of finite resolution are not considered in the analysis.

The intensity and interferometric coherence coefficient of the streaks along line AZ are higher across the surf zone (Fig. 4, range 100–250 m) than in the region seaward of breaking waves (range $>$ 250 m). The streak length is estimated as the distance over which the power is 3 dB above the backscattered signal from a surface without breaking waves. Assuming that all waves of a given height break the same distance from the shoreline (line AB in Fig. 3), streak lengths (Fig. 4 shows an example) are averaged along azimuthal lines (e.g., AZ in Fig. 3) separated by 2 m (the slant range resolution) within a trapezoidal area (ABZZ' in Fig. 3) near the shoreline to obtain a mean streak length. The mean length of the streaks is about 110 to 120 m, corresponding to a mean bandwidth of radial velocities of 2.4–2.7 m/s, consistent with surface velocities associated with breaking waves in the surf zone.

## V. Analysis Of Experimental Data

The radial velocity bandwidth estimated with ATI SAR and the significant wave height estimated with *in situ* sensors are correlated well (correlation coefficient $r^2 = 0.78$; Fig. 5). The angle of wave arrival does not appear to affect the relationship for the range of the observed wave heights $30 < H_{\text{sig}} < 70$ cm. A least squares fit of the observed significant wave height to the radial velocity bandwidth ($\Delta V_r$) (Fig. 5 black line) yields

$$H_{\text{sig}} = 23.58\Delta V_r + 2.33. \tag{3}$$

The total power of the microwave signal scattered from breaking waves also can be related to the height of the waves. However, the ratio of power scattered from waves with $H_{\text{sig}} =$ 30 cm to the power for $H_{\text{sig}} = 70$ cm is less than about 10, and thus, a good fit requires a more accurate calibration of the intensity than is available in these data.

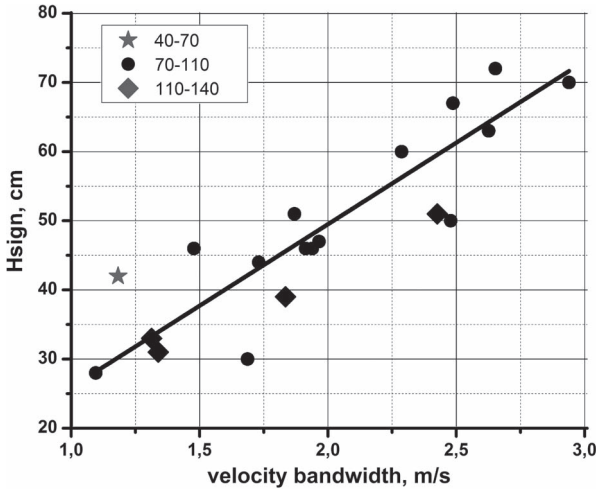


Fig. 5. Observed significant wave height versus SAR inferred radial velocity bandwidth for waves from 40°–70° (stars), 70°–100° (circles), and 110°–140° (squares). Waves propagating perpendicular to the shoreline (normally incident) are from 90° in this coordinate system. The black line is the least squares linear fit to all of the data.

## VI. Modeling

A phase-resolving Boussinesq wave model for cross-shore propagation of regular ocean surface waves on a planar seabed [10], [11] is used to verify the relationship derived between *in situ* estimates of $H_{\text{sig}}$ and SAR estimates of radial velocity [Fig. 5 and (3)]. The input parameters for the model are the measured slope of the seafloor (0.02 [12]) and representative incident wave heights and wave periods. The model simulates the evolution of waves as they propagate across the shoaling and breaking regions (Fig. 6).

The SAR forms an image from continuous observation of the area of interest over a time period given by the distance to the observed area $R$ multiplied by the antenna beam width $\beta$ divided by the velocity of the platform $V$ [9]. Assuming an average $R$ of 2–3 km, a probability density function is estimated for the simulated surface velocities of breaking waves (Fig. 7) spanning the surf zone (boxed region in Fig. 6) over the expected 5–10-s observation period. Only velocities identified by the model as being associated with breaking waves were used to generate the density function.

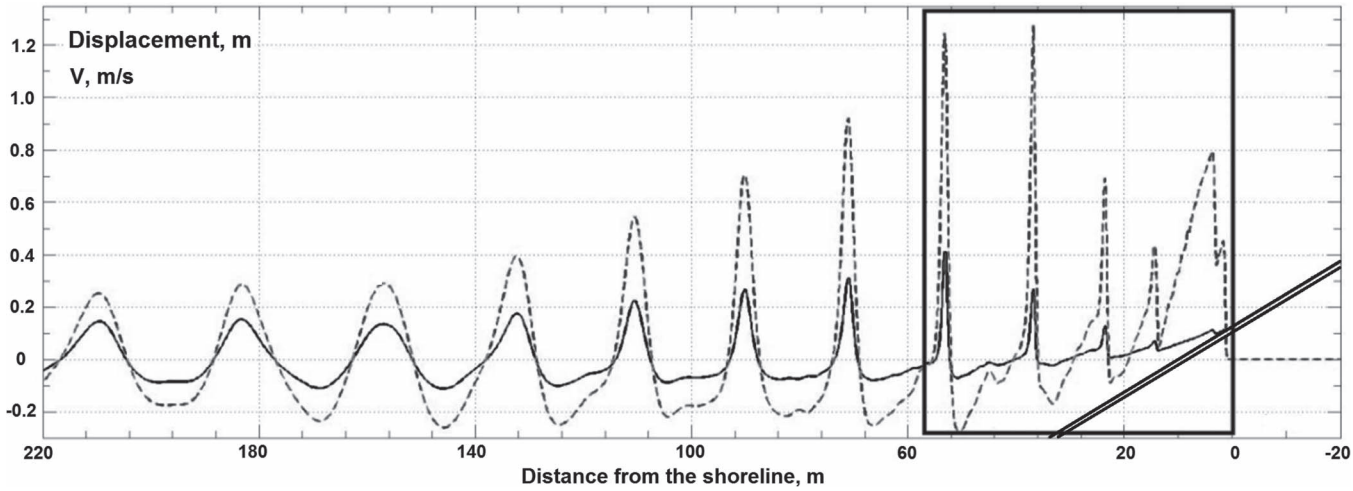


Fig. 6. Simulated sea-surface elevation (solid curve) and orbital velocity (dashed) versus distance from the shoreline. The incident significant wave height was 0.32 m. The boxed region indicates the surf zone, and the thick angled line centered on $x = 0$ m is the seafloor.

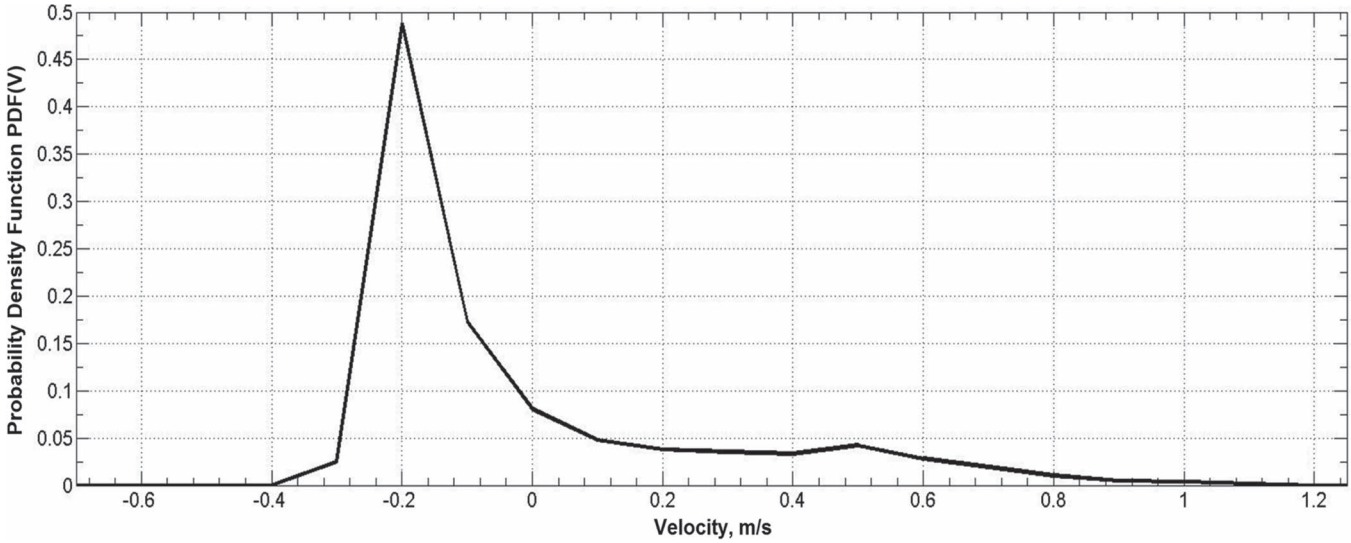


Fig. 7. Probability density function of simulated velocity (m/s) estimated for breaking waves in the surf zone (boxed region in Fig. 6) with incident significant wave height 0.32 m.

The simulated distribution does not contain any noise, and thus, the bandwidth is defined as the range over which the distribution is nonzero. In this case, the maximal negative and positive velocities are $-0.4$ and 1.2 m/s (Fig. 7), respectively, so the velocity bandwidth for these simulated waves is equal to 1.6 m/s. In contrast to the SAR-based method, which uses the image intensity as a function of along-azimuth distance to estimate streak lengths (Fig. 4) that are then used to estimate the velocity bandwidth, this model-based method estimates the velocity bandwidth directly from the simulations (Fig. 7).

The velocity bandwidth was estimated from simulated waves with initial significant wave heights from 30 to 80 cm, spanning the range of observed values. The relationship between simulated wave heights and velocity bandwidth is similar to that between *in situ*-based wave heights and SAR-estimated velocity bandwidths (Fig. 8). The Pearson correlation coefficient $(=0.82)$ calculated from the cosine of the angle between regression lines for experimental and simulated data suggests that the two data sets come from the same statistical population.

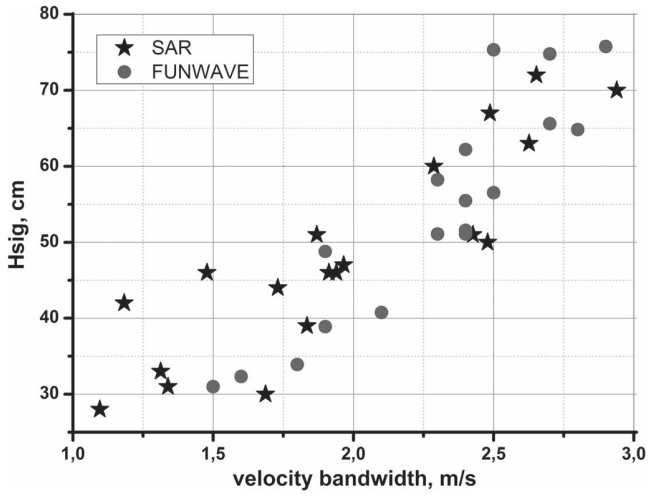


Fig. 8. Simulated significant wave height versus radial velocity bandwidth (blue symbols). The red symbols are the *in situ*-estimated wave heights versus SAR-estimated velocity bandwidths shown in Fig. 4.

## VII. Conclusion

An empirical relationship between ocean observations of waves and radial velocity bandwidths estimated from SAR images has skill estimating breaking-wave heights in the surf zone. The approach was verified with numerical simulations of breaking waves. The relationship appears to be robust for a range of wave conditions observed for one month in the nearshore region near an inlet in the Atlantic Ocean. Application of the technique to estimate numerically simulated breaking-wave heights suggests that it may have skill at other sites.

## Acknowledgment

The authors would like to thank the PVLAB field crew for helping in obtaining the ocean observations in less than ideal conditions and the staff of the USACE FRF for the logistical support and bathymetry.

## References

[1] M. Marom, L. Shemer, and E. B. Thornton, "Energy density directional spectra of a nearshore wave field measured by interferometric synthetic aperture radar," *J. Geophys. Res.*, vol. 96, pp. 22 125–22 134, 1991.

[2] P. A. Hwang, J. V. Toporkov, M. A. Sletten, and S. P. Menk, "Mapping surface currents and waves with interferometric synthetic aperture radar in coastal waters: Observations of wave breaking in swell-dominant conditions," *J. Phys. Oceanogr.*, vol. 43, no. 3, pp. 563–582, Mar. 2013.

[3] J. V. Toporkov, "Analytical study of along-track InSAR imaging of a distributed evolving target with application to phase and coherence signatures of breakers and whitecaps," *IEEE Geosci. Remote Sens. Lett.*, vol. 11, no. 8, pp. 1385–1389, Aug. 2014.

[4] D. T. Walker, C. Wackerman, and E. Ericson, "Estimating breaker height and type in the surf zone using SAR," in *Proc. IEEE Int. Geosci. Remote Sens. Symp.*, 1998, vol. 3, 1394–1396.

[5] G. Farquharson, D. Huazeng, Yu. Goncharenko, and J. Mower, "Dual-beam ATI SAR measurements of surface currents in the nearshore ocean," in *Proc. IEEE Int. Geosci. Remote Sens. Symp.*, 2014, pp. 2661–2664.

[6] J. Chen, T. Hsu, F. Shi, B. Raubenheimer, and S. Elgar, "Hydrodynamic and sediment transport modeling of New River Inlet (NC) under the interaction of tides and waves," *J. Geophys. Res.*, to be published.

[7] H. Shi, X. Guo, and Y. Zhou, "Study on the signature of ground moving target for airborne squint SAR imaging," *J. Electron. (China)*, vol. 29, no. 6, pp. 477–484, Nov. 2012.

[8] M. L. Schwartz, *Encyclopedia of Coastal Science*. Dordrecht, The Netherlands, Springer-Verlag, 2005.

[9] D. R. Lyzenga and R. A. Shuchman, "Analysis of scatterer motion effects in Marsen X band SAR imagery," *J. Geophys. Res.*, vol. 88, no. C14, pp. 9769–9775, Nov. 1983.

[10] F. Shi *et al.*, "A high-order adaptive time-stepping TVD solver for Boussinesq modeling of breaking waves and coastal inundation," *Ocean Model.*, vol. 43/44, pp. 36–51, Dec. 2011.

[11] F. Shi, J. T. Kirby, B. Tehranirad, J. C. Harris, and S. T. Grilli, "FUNWAVE-TVD, Fully Nonlinear Boussinesq Wave Model With TVD solver, documentation and user's manual," Center Appl. Coastal Res., Univ. Delaware, Newark, DE, USA, Res. Rep. No CACR-11-04 V2.1, 2011.

[12] Field Research Facility. Coastal & Observation Branch. [Online]. Available: http://www.frf.usace.army.mil/nri/